

# Phase transformation and microstructural evolution after heat treatment of a terbium-doped lithium–aluminum phosphate glass

Roque S. Soares · Regina C. C. Monteiro ·  
Maria M. R. A. Lima · Bogdan A. Sava ·  
Mihail Elisa

Received: 28 December 2013 / Accepted: 11 March 2014 / Published online: 28 March 2014  
© Springer Science+Business Media New York 2014

**Abstract** The crystallization kinetics and phase transformation of a transparent Tb<sup>3+</sup>-doped lithium–aluminum phosphate glass, prepared by melt quenching, were investigated. The energy associated to the glass transition and the crystallization parameters (activation energy for crystallization and Avrami exponent) were evaluated by different methods using the experimental data obtained by differential thermal analysis performed at different heating rates. Using an isoconversional method to determine the change of the activation energy for crystallization with the fraction of crystallization, it was verified that with the increase in the fraction of crystallization from 0.1 to 0.9, the value of the activation energy decreased slightly from ~370 to ~310 kJ mol<sup>-1</sup> and that the Avrami exponent varied from 0.8 to 1, suggesting a surface crystal growth mechanism. Observation of the microstructural evolution of heat-treated glass samples confirmed a surface crystallization process revealing spherulitic crystals constituted mainly by aluminum metaphosphate.

## Introduction

In recent years, phosphate-based glasses have attracted renewed interest because of their potential use in a great variety of optical devices. Moreover, phosphate-based glasses have shown interesting physical and chemical properties that make them attractive as hosts for luminescent ions [1]. Studies on glasses doped with rare-earth (RE) ions have attracted a great interest for the reason that the particular 4f electronic configuration of the RE ions in a variety of glass matrices leads to emissions from ultraviolet to infrared [2, 3] conducting to many potential applications, such as fluorescent lamps, two-dimensional X-ray sensors, solar control devices, solid laser, and optical amplifiers [4–6]. Therefore, Tb-doped lithium aluminum phosphate glasses have great potential for the above applications [7, 8].

Production of optical glasses with high RE oxide content involves considerable technological difficulties caused by the increased crystallization ability, amorphous phase separation phenomena, and high melting temperatures. High thermal stability and transparency of the lithium–aluminum phosphate glasses constitute also underlying properties for the exploitation of these host materials in photonics and optoelectronics applications. Transparency is generally lost after the heat treatment of a glass at high temperature due to the growth of crystallites into large crystals, which results in increased scattering of light caused by the difference in the refractive index between the glass matrix and the precipitated crystals [9]. However, the devitrified glass can show transparency when very fine crystals are precipitated, and such transparent glass–ceramics have been developed and partially used in many application fields [10].

The structural and optical characteristics of RE-doped aluminophosphate glasses have been studied by some of the authors of the present work [4–6]. However, the crystallization

---

R. S. Soares · R. C. C. Monteiro (✉) · M. M. R. A. Lima  
Department of Materials Science, CENIMAT/I3N, Faculty of  
Sciences and Technology, Universidade Nova de Lisboa,  
2829-516 Caparica, Portugal  
e-mail: rcm@fct.unl.pt

R. S. Soares  
e-mail: roque.saldanha.soares@gmail.com

M. M. R. A. Lima  
e-mail: mmal@fct.unl.pt

B. A. Sava · M. Elisa  
Department of Optospintronics, National Institute of R & D for  
Optoelectronics, INOE 2000, 77125 Magurele, Romania  
e-mail: savabogdanalexandru@yahoo.com

M. Elisa  
e-mail: astatin18@yahoo.com

behavior in these glass systems has generally not been reported, and up to now, there is little information on the thermal transformation and crystallization kinetics of multi-component aluminophosphate glasses [11]. The ability to control the crystallization of different vitreous matrices permits the glass synthesis under ideal conditions. The understanding of the mechanism of crystallization is essential for most of the glass applications, as stability against crystallization determines the effective working limits [11]. In order to obtain a fine microstructure and transparency in heat-treated glasses, an intensive nucleation effect is essential. Parameters that are of utmost interest include the kinetic parameters, activation energy of crystallization,  $E_c$ , and Avrami exponent,  $n$ , the last one providing the possibility to determine the mechanisms of the nucleation and growth processes.

Differential thermal analysis (DTA) and differential scanning calorimetry (DSC) have been frequently used to investigate the glass transition and the kinetics of crystallization of glassy materials [12, 13]. Thermally activated transformations in the solid state can be investigated by calorimetric measurements using two basic methods: isothermal and non-isothermal [14].

The crystallization kinetics has been studied using the formal theory of transformation kinetics proposed by the Johnson–Mehl–Avrami (JMA) model [15–17]. The JMA model is valid only under isothermal conditions. However, isothermal experiments are generally very time-consuming, while experiments performed at constant heating rate enable a more expeditious gathering of the experimental data. Besides, the impossibility of instantaneously reaching the testing temperature under “isothermal” conditions means that no measurements are possible while the system is approaching the set temperature. Constant heating rate experiments do not have this drawback [14].

The purpose of the present study was to investigate the phase transformation and the non-isothermal crystallization kinetics of a  $Tb^{3+}$ -doped lithium–aluminum phosphate glass. The activation energy for crystallization, rate of crystallization, and dimensionality of the crystal growth were estimated by different methods using non-isothermal DTA data obtained at constant heating rates. X-ray diffraction (XRD) was used to identify the crystalline phases that were present in heat-treated glass samples, and optical microscopy and scanning electron microscopy (SEM) were used to investigate the microstructural evolution.

## Experimental procedure

### Preparation of the glass samples

The glass, with a nominal composition 20.48  $Li_2O$ -7.23  $BaO$ -10.24  $Al_2O_3$ -1.45  $La_2O_3$ -58.43  $P_2O_5$ -2.17  $Tb_2O_3$

(mol%), was prepared from analytical grade reagents,  $Li_2CO_3$ ,  $BaCO_3$ ,  $Al_2O_3$ ,  $La_2O_3$ ,  $H_3PO_4$ , and  $Tb_2O_3$ , using a wet non-conventional raw materials preparation followed by melt quenching of the glass. Details of similar preparation procedure adopted for aluminophosphate glasses doped with different RE ions have been reported elsewhere [18].

First, the raw materials were added to a  $H_3PO_4$  solution, mixed by continuous stirring, and then the mixture was heated and dried on a heating plate until the batch viscosity was significantly increased. This homogenization and drying step is accompanied by the release of gasses resulting from chemical reactions that promote the formation of homogeneous metaphosphates improving the chemical homogeneity of the final glass [18].

Subsequently, the dried mixture was heat treated in an alumina crucible during two sequential steps: (i) at a heating rate of  $100\text{ K h}^{-1}$  from room temperature up to 973 K, to eliminate volatile components, and (ii) at a heating rate of  $250\text{ K h}^{-1}$  up to 1,523 K with 4 h holding at this temperature to achieve glass melting and refining. Then, the glass was cast in graphite molds, and annealed at 723 K for 6 h to remove internal stresses.

The as-prepared glass block was cut with a diamond disk to obtain thin glass slabs with a thickness of about 2 mm, that were polished using 150, 300 and 600 grade SiC followed by CEROX abrasive. Powder samples for the thermal analysis were prepared from small fragments of the glass that were milled in an agate mortar and pestle to obtain a glass powder with the particle size smaller than  $65\text{ }\mu\text{m}$ . The heat-treated samples used in this study were prepared by heating small plate-shaped glass samples ( $\sim 7\text{ mm} \times 7\text{ mm} \times 2\text{ mm}$ ) in an electric tubular furnace at a heating rate of  $10\text{ }^\circ\text{C min}^{-1}$  from room temperature up to a selected temperature, suggested by the DTA results, and held at that temperature for various times.

### Characterization methods

DTA was performed in an equipment (STA PT 1600, Linseis, Germany), interfaced with a computerized data acquisition and analysis system. Samples of glass powder (50 mg) were heated inside an alumina crucible, in static air, from room temperature up to a maximum temperature of 973 K, at various heating rates (10, 15, 20, 25, and  $30\text{ K min}^{-1}$ ). From the DTA curves, the glass transition temperature ( $T_g$ ), the onset crystallization temperature ( $T_i$ ), and the maximum crystallization temperature ( $T_p$ ) were determined.

To confirm the amorphous nature of the as-prepared glass and to identify the crystalline phases formed in heat-treated glass samples, XRD analyses were performed in a diffractometer (Dmax III-C 3 kW, Rigaku Corporation,

Tokyo, Japan) using Cu K $\alpha$  radiation ( $\lambda = 1.5406$  nm) produced at 40 kV and 30 mA, a scanning range of diffraction angles ( $2\theta$ ) between  $10^\circ$  and  $60^\circ$ , and an acquisition time of 1s and  $2\theta$  increment of  $0.04^\circ$ . The crystalline phases were identified by comparing the peak positions and intensities with those listed in the software standard files (ICDD, Newtown Square, PA, USA).

Microstructural observations were carried out with a polarization optical microscope (Olympus-BX51 TRF, USA) and with a scanning electron microscope (SEM–FIB–Zeiss Auriga, Germany) using glass samples and heat-treated glass samples. In order to reduce the charge effects, as the samples are nonconductive, the deposition of a 4 nm Au/Pd was performed immediately before SEM observations. Energy dispersive spectroscopy (EDS, Oxford INCA Energy 350) was employed for elemental chemical analysis.

**Results**

DTA curves for the glass obtained at different heating rates (10, 15, 20, 25, and 30 K min<sup>-1</sup>) are presented in Fig. 1. A well-defined endothermic peak corresponds to the glass

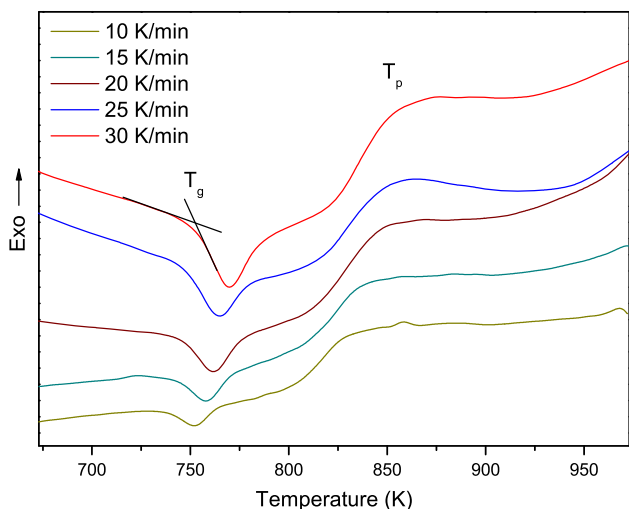


**Fig. 1** DTA thermographs for glass powder at various heating rates

**Table 1** Values of glass transition temperature ( $T_g$ ) and of peak crystallization temperature ( $T_p$ ) for the various heating rates ( $\beta$ ). Values of activation energy associated with glass transition ( $E_g$ ) of

$\beta$ (K min <sup>-1</sup> )	$T_g$ (K)	$T_p$ (K)	$E_g$ (kJ mol <sup>-1</sup> )	$E_c$ (kJ mol <sup>-1</sup> )	$n$
10	741	834	$462 \pm 14$ Eq. (2)	$262 \pm 14$ Eq. (5)	1.02
15	745	843			
20	748	851	$475 \pm 14$ Eq. (3)	$276 \pm 14$ Eq. (6)	0.97
25	749	856			
30	751	858			

transition region, and the temperature at which the tangents intersect (see Fig. 1) is the glass transition temperature ( $T_g$ ). Each DTA curve exhibits a broad exothermic peak associated to the glass crystallization with a maximum crystallization peak temperature ( $T_p$ ). The values of  $T_g$  and of  $T_p$  for the different heating rates ( $\beta$ ) are summarized in Table 1.

**Glass transition analysis**

The glass transition temperature ( $T_g$ ) was related with the heating rate ( $\beta$ ) according to Lasocka’s empirical relation [19]

$$T_g = A_g + B_g \log \beta, \tag{1}$$

where  $A_g$  and  $B_g$  are the constants for a given glass composition. Figure 2 shows the change of  $T_g$  as a function of  $\log \beta$ , a straight regression line fitted to the experimental data and Eq. (1) written for the particular case of this glass.

A second approach to analyze the dependence of  $T_g$  on  $\beta$ , which is commonly used to estimate the activation energy associated with the glass transition ( $E_g$ ) under non-isothermal treatment schedules, was based on Kissinger’s equation, that may be written as follows [20, 21]:

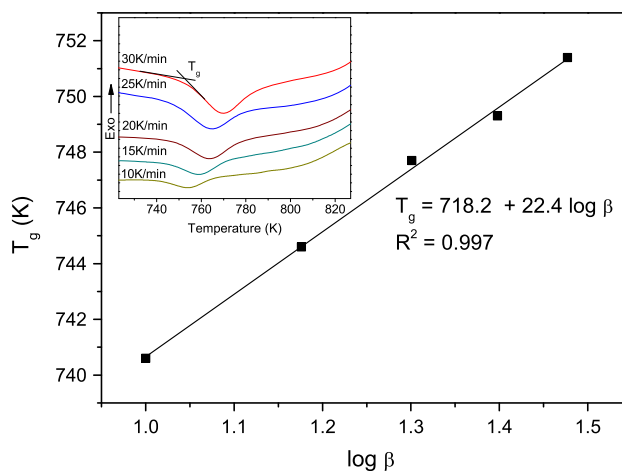


**Fig. 2** Change of  $T_g$  with  $\log \beta$ . The inset depicts the DTA endothermic peak observed at various heating rates

activation energy for crystallization ( $E_c$ ) calculated according to different methods and of Avrami exponent ( $n$ ) are also shown

$$\ln\left(\frac{\beta}{T_g^2}\right) = -\frac{E_g}{RT_g} + \text{const}, \quad (2)$$

where  $R$  is the universal gas constant. Figure 3 shows the variation of  $\ln\left(\beta/T_g^2\right)$  with  $(1,000/T_g)$ . From the slope of the straight regression line fitted to the experimental data, the value of  $E_g$  was calculated ( $462 \pm 14 \text{ kJ mol}^{-1}$ , see Table 1).

Another approach can be used to calculate  $E_g$ , assuming that the variation of  $\ln\left(1/T_g^2\right)$  with  $\ln\beta$  is much slower than that of  $\ln(1/T_g)$  with  $\ln\beta$  [21]. So, the Kissinger equation can be simplified in the following form [21]:

$$\ln\beta = -\frac{E_g}{RT_g} + \text{const}. \quad (3)$$

The change of  $\ln\beta$  as a function of  $1,000/T_g$  is also shown in Fig. 3, and the value of  $E_g$  calculated from the slope of the line fitted to the data ( $475 \pm 14 \text{ kJ mol}^{-1}$ ) is also presented in Table 1.

### Glass crystallization analysis

The peak temperature of crystallization ( $T_p$ ) for the glass was related to the heating rate ( $\beta$ ), considering as well Lasocka's empirical relation [19] in the following way:

$$T_p = A_p + B_p \log \beta, \quad (4)$$

where  $A_p$  corresponds to the peak temperature of crystallization at the heating rate  $1 \text{ K min}^{-1}$ , and  $B_p$  is a constant for a given glass composition [19]. Figure 4 shows the change of  $T_p$  with  $\log\beta$  (the solid line is a linear regression fit) and Eq. (4) written for the particular case of the present glass.

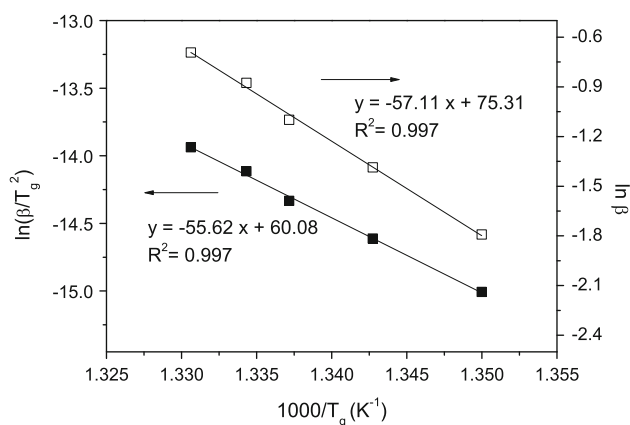


**Fig. 3** Changes of  $\ln\left(\beta/T_g^2\right)$  and of  $\ln\beta$  with  $1,000/T_g$

The activation energy for crystallization ( $E_c$ ) was evaluated through the variation of  $T_p$  with  $\beta$  according to the equation formulated by Kissinger [20] that is widely used for analyzing crystallization during DTA experiments:

$$\ln\left(\frac{\beta}{T_p^2}\right) = -\frac{E_c}{RT_p} + \text{const}. \quad (5)$$

A plot of  $\ln\left(\beta/T_p^2\right)$  versus  $1,000/T_p$  for the crystallization peak of the DTA curve is shown in Fig. 5. The value of  $E_c$  calculated from the slope of the straight regression line fitted to the DTA experimental data ( $262 \pm 14 \text{ kJ mol}^{-1}$ ) is presented in Table 1. Taking into account that the change in  $\ln\left(1/T_p^2\right)$  with  $\ln\beta$  is negligibly small compared with the change of  $\ln\left(1/T_p\right)$  with  $\ln\beta$ , it is possible to write Eq. (5) in a simplified form [21, 22] as follows:

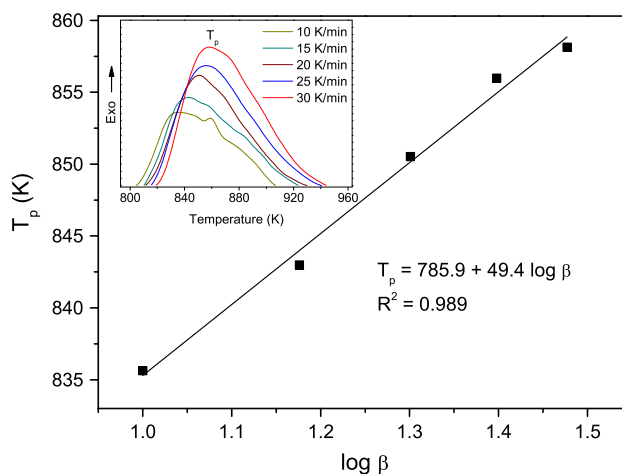


**Fig. 4** Change of  $T_p$  with  $\log\beta$ . The inset depicts the DTA exothermic peak observed at various heating rates

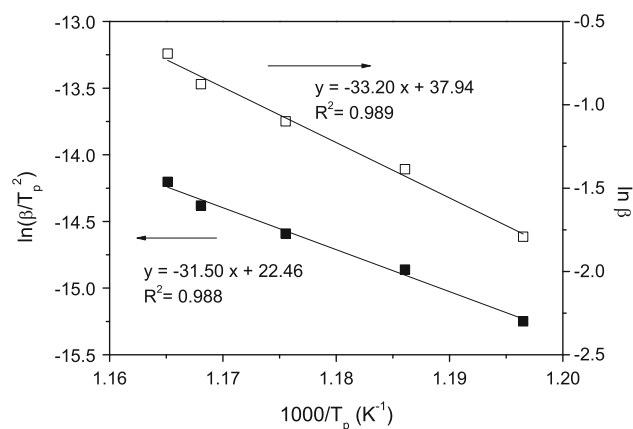


**Fig. 5** Changes of  $\ln\left(\beta/T_p^2\right)$  and of  $\ln\beta$  with  $1,000/T_p$

$$\ln \beta = -\frac{E_c}{RT_p} + \text{const.} \tag{6}$$

From the linear plot of  $\ln \beta$  versus  $1/T_p$ , also shown in Fig. 5, it was possible to calculate the value of  $E_c$  ( $276 \pm 14 \text{ kJ mol}^{-1}$ ), which is also presented in Table 1.

The fraction of crystallization ( $\chi$ ) at a selected temperature ( $T$ ) was determined from the DTA curve obtained at a specific heating rate [21, 23]. The value of  $\chi$  at a given temperature ( $T$ ) is determined by the ratio  $A_T/A$  [21, 23], where  $A$  is the total area of the exotherm peak between the temperature  $T_i$  (where crystallization just begins) and the temperature  $T_f$  (where the crystallization is completed), as shown schematically in Fig. 6; and  $A_T$  is the area between  $T_i$  and  $T$  (temperature selected between  $T_i$  and  $T_f$ ). The graphical representation of the volume fraction crystallized ( $\chi$ ) as a function of temperature ( $T$ ) for all the used heating rates is shown in Fig. 7.

The crystallization rate ( $d\chi/dt$ ) at any temperature ( $T$ ) has been determined from the ratio between the corresponding ordinate of the DTA curve and the total area of the crystallization peak [24], and the change of the crystallization rate ( $d\chi/dt$ ) as a function of  $T$  for the present glass is shown in Fig. 8. From the experimental values of the crystallization rate at the peak temperature of crystallization,  $(d\chi/dt)_{T_p}$ , it is possible to calculate the kinetic exponent ( $n$ ) according to the following equation [23, 24]:

$$n = \left(\frac{d\chi}{dt}\right)_{T_p} \frac{RT_p^2}{0.37\beta E_c} \tag{7}$$

The kinetic exponent  $n$  at each experimental heating rate was evaluated according to the above equation, considering

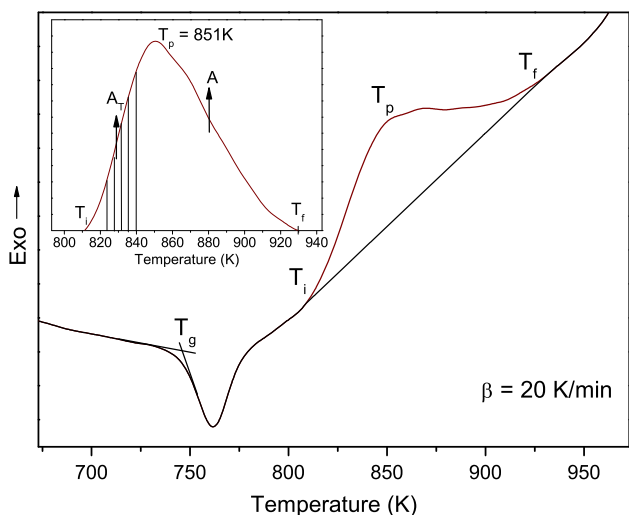


**Fig. 6** Lined area  $A_T$  between  $T_i$  and  $T$  and area  $A$  between  $T_i$  and  $T_f$  for the crystallization peak at the heating rate of  $20 \text{ K min}^{-1}$ .  $T_i$ ,  $T_f$ , and  $T$  according to the text

the values of  $E_c$  determined according to Eqs. (5) and (6), and the mean value was  $\langle n \rangle = (1.02 \pm 0.08)$  and  $(0.97 \pm 0.07)$ , respectively (see Table 1).

According to the modified Ozawa equation [25], in non-isothermal crystallization, the volume fraction of crystallites ( $\chi$ ) precipitated in a glass heated at constant rate ( $\beta$ ) is related to the crystallization activation energy ( $E_c$ ) through the following expression:

$$\ln[-\ln(1-\chi)] = -n \ln \beta - 1.052(n-1)(E_c/RT) + \text{const.} \tag{8}$$

The variation of  $\ln[-\ln(1-\chi)]$  with  $1,000/T$  for all the heating rates was determined and shown to be non-linear (see Fig. 9). Therefore, it is suggested that there is a variation of  $E_c$  and of  $n$  during the crystallization process [26].

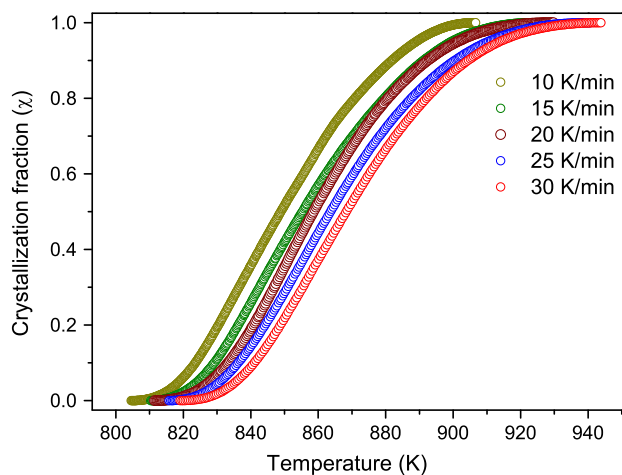


**Fig. 7** Crystallization fraction ( $\chi$ ) as a function of temperature for different heating rates

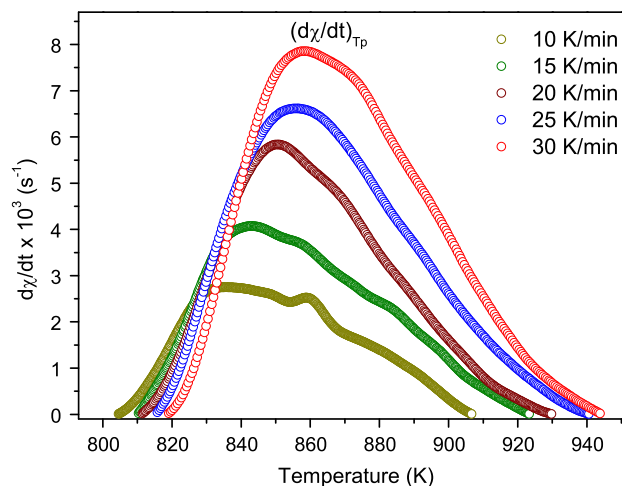


**Fig. 8** Crystallization rate as a function of temperature for the different heating rates

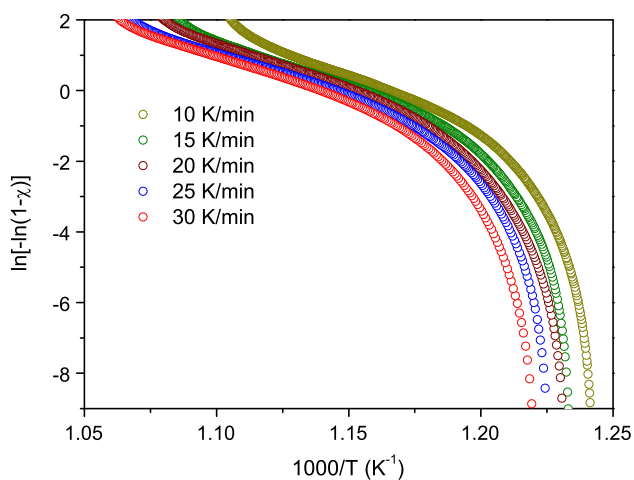


**Fig. 9** Change of  $\ln[-\ln(1-\chi)]$  with  $1,000/T$  for the various heating rates

The effective activation energy,  $E_c(\chi)$ , that represents the activation energy at a stage when the crystallized volume fraction is  $\chi$ , was determined by an isoconversional method [27, 28], based on the method proposed by Kissinger [20], and according to the following expression:

$$\left[ \frac{d \ln(\beta/T_p^2)}{d(1/T)} \right]_{\chi} = -\frac{E_c(\chi)}{R}, \tag{9}$$

where  $R$  is the gas constant,  $T_p$  is the peak crystallization temperature, and  $T$  and  $\beta$  are the temperature and the heating rate, respectively, corresponding to the value of  $\chi$ .

Using the experimental data that are depicted in Fig. 7, plots of  $\ln(\beta/T_p^2)$  versus  $1,000/T$  were obtained for various values of  $\chi$ ,  $0.1 < \chi < 0.9$  (Fig. 10a), and the values of  $E_c(\chi)$  were calculated from the slope of the straight regression lines fitted to the experimental data for the various  $\chi$ . Similarly,  $E_c(\chi)$  values were estimated on the basis of the method proposed by Ozawa [22], using the following equation:

$$\left[ \frac{d \ln(\beta)}{d(1/T)} \right]_{\chi} = -\frac{E_c(\chi)}{R}. \tag{10}$$

Plots of  $\ln\beta$  as function of  $1,000/T$  were obtained for the various values of  $\chi$  in the same range,  $0.1 < \chi < 0.9$  (Fig. 10b), and  $E_c(\chi)$  values were determined from the slope of the lines fitted to the experimental data for the various  $\chi$ . Figure 11 illustrates the change of  $E_c(\chi)$  with the crystallized volume fraction ( $\chi$ ).

Taking into account the values of effective activation energy,  $E_c(\chi)$ , determined according to Kissinger and Ozawa methods, the values of Avrami exponent,  $n(\chi)$ , for the various heating rates (10, 15, 20, 25, and 30 K/min) were calculated using the following equation [29]:

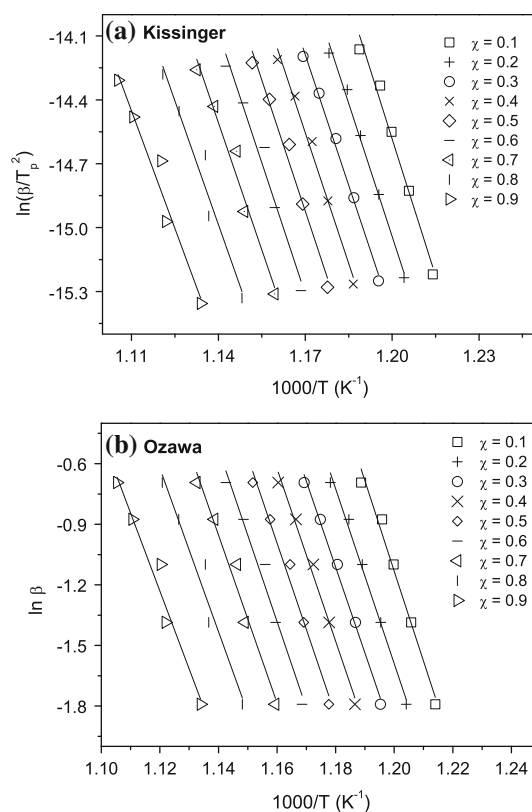


**Fig. 10** Changes of **a**  $\ln(\beta/T_p^2)$  and **b**  $\ln\beta$  with  $1,000/T_p$  for  $E_c(\chi)$  determination by Kissinger and Ozawa methods, respectively

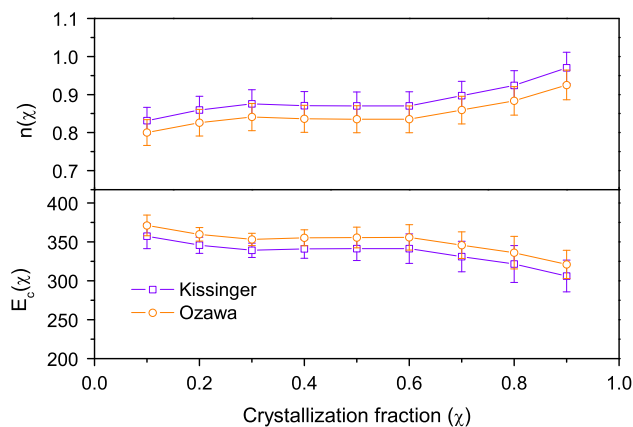


**Fig. 11** Plot of effective activation energy for crystallization,  $E_c(\chi)$ , and of Avrami exponent,  $n(\chi)$ , as a function of crystallization fraction ( $\chi$ )

$$n(\chi) = \frac{-R}{E_c(\chi)} \frac{\partial \ln[-\ln(1-\chi)]}{\partial \ln(1/T)}. \tag{11}$$

Figure 11 shows the variation of the Avrami exponent with the fraction of crystallization ( $\chi$ ).

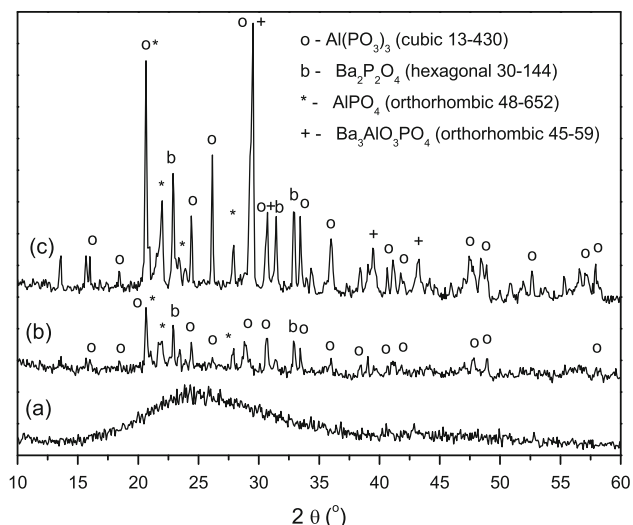


**Fig. 12** XRD patterns of **a** glass and of the glass heat treated at **b** 733 K for 8 h plus 773 K for 2 h and **c** at 733 K for 8 h plus 873 K for 2 h

#### Crystalline phases and microstructural analysis

XRD analysis confirmed that the as-prepared glass was fully amorphous, see Fig. 12a. The XRD patterns for glass samples heat treated during 8 h at 733 K and then heated for 2 h at 773 and at 873 K are presented in Fig. 12b, c respectively. Aluminum metaphosphate,  $\text{Al}(\text{PO}_3)_3$ , was identified as the predominant phase, together with aluminum phosphate ( $\text{AlPO}_4$ ), and also barium phosphate ( $\text{Ba}_2\text{P}_2\text{O}_7$ ) and barium-aluminum phosphate, ( $\text{Ba}_3\text{AlPO}_7$ ) as minor phases.

Figure 13 presents the optical microscopy images under cross-polarized light of the glass and of two glass samples after different heat treatment schedules. A detailed microstructural observation was performed by SEM, and Fig. 14 shows the SEM micrographs for glass samples treated under different conditions. This observation was complemented by EDS analysis with elemental mapping in some of the heat-treated glass samples (see Fig. 15).

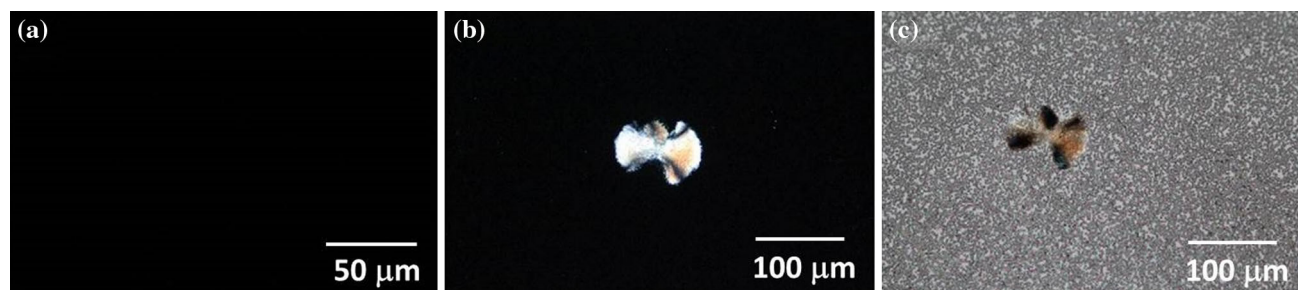


**Fig. 13** Optical microscope images under crossed-polarized light of **a** glass and of the glass heat treated at **b** 733 K for 8 h plus 773 K for 2 h and **c** at 733 K for 8 h plus 873 K for 2 h

## Discussion

### Glass transition

The straight regression line fitted to the experimental data in the plot of  $T_g$  versus  $\log\beta$  (Fig. 2) represents the validity of the dependence of the glass transition temperature on the heating rate given by Eq. (1). According to this equation, the value of  $A_g$  corresponds to the glass transition temperature for a heating rate of  $1 \text{ K min}^{-1}$ . It has been suggested that the parameter  $B_g$  is dependent on the method of quenching the glass, the lower the cooling rate of the melt, the lower the  $B_g$  value [21]. The inset in Fig. 2 clearly shows an upward shift of the endothermic peak with the increase of the heating rate. The systematic shift in the peak position with the heating rate has been tentatively attributed to a thermal relaxation phenomenon [12]. The glass transition temperature ( $T_g$ ) of a multi-component glass is known to be dependent on several independent parameters such as co-ordination numbers, bond energy, effective molecular weight, type, and fraction of the various structural units that are formed [30]. The glassy solid state is characterized by very slow relaxation kinetics due to the relatively high viscosity, which makes difficult the local arrangement of the bonds and the atomic displacements. This type of thermal relaxation depends upon the thermal treatment and may be quite fast near  $T_g$ . Thus, it is reasonable to associate  $T_g$  with the glass structural rearrangements, a phenomenon that requires an activation energy [30, 31].

The activation energy for glass transition is considered as the amount of energy that is absorbed by a group of atoms in the glassy region so that a jump from one metastable state to another is possible [32]. The activation energy for glass transition ( $E_g$ ) under non-isothermal treatment conditions was estimated by both Kissinger's equation [20] and its simplified form [21, 22]. Although these equations were originally deduced for the crystallization process, they have been frequently used to calculate the activation energy for glass transition [21], which

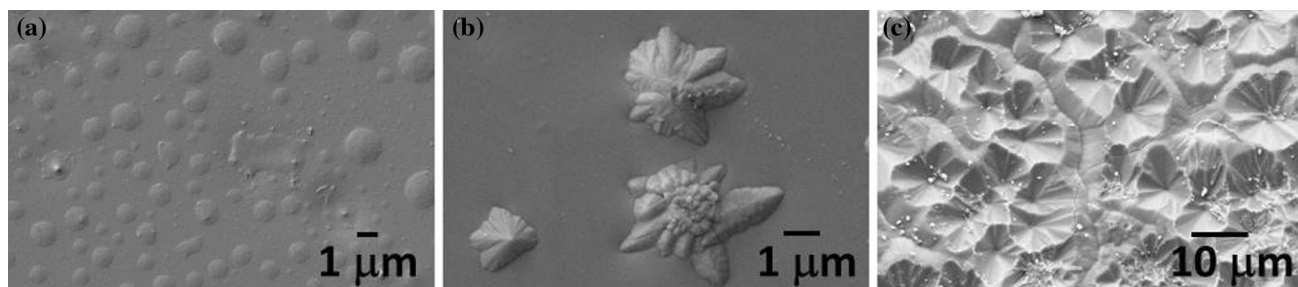


**Fig. 14** SEM images of glass samples heat treated at **a** 733 K for 8 h, **b** 733 K for 8 h plus 773 K for 2 h, and **c** at 733 K for 8 h plus 873 K for 2 h

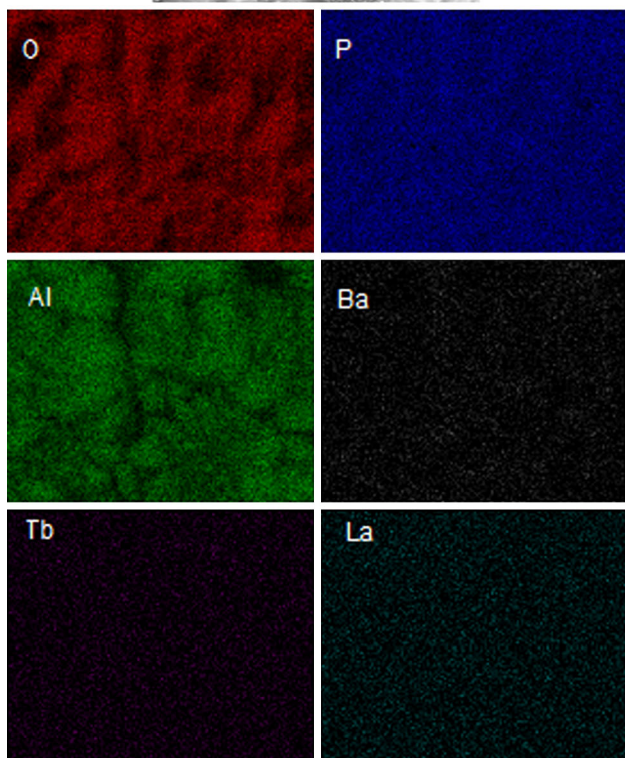
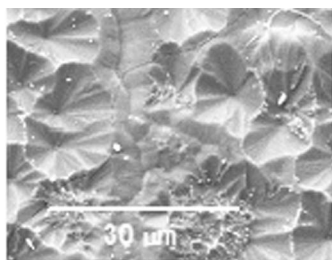


**Fig. 15** SEM image and EDS element mapping of O, P, Al, Ba, La, and Tb after heat treatment at 733 K for 8 h followed by 873 K for 2 h

involves the molecular motion and rearrangement of atoms around  $T_g$  [32, 33]. It is verified that the values calculated for  $E_g$ , which are present in Table 1, are in close agreement, the discrepancy between the values being consistent with the difference between Eq. [2] and Eq. [3].

### Crystallization kinetics

From the results presented in Table 1, it is observed that the peak crystallization temperature ( $T_p$ ) increases with the increase in the heating rate and that the difference between  $T_p$  and  $T_g$  increases from 93 to 107 K when the heating rate increases from 10 to 30 K min<sup>-1</sup>. The maximum crystallization in DTA curves corresponds to the temperature at which the rate of transformation of the viscous liquid into crystals becomes the maximum. When the crystalline phase has the same composition as that of the liquid, the rate of the transformation will depend on the density of the crystallization sites. However, when the composition of the crystalline phase is different from that of the liquid, as in the present case (cf. XRD results in Fig. 12), the rate of transformation will be controlled by the rate of diffusion through the viscous liquid and the number of crystallization sites into which diffusion can occur. If the number of nucleation sites is increased, e.g., using slower heating rates, the peak maximum will occur at a temperature at which the melt viscosity is higher, i.e., at lower temperature. This explains the increase in  $T_p$  with the heating rate as observed in the present study (see Table 1; Fig. 4).

By monitoring the shift in the position of the exothermic peak as a function of the heating rate, it has been possible to determine the kinetic parameters of the glass crystallization [12, 21–25]. Taking into account the results presented in Table 1, it is observed that the values of  $E_c$  determined according to Eqs. (5) and (6),  $262 \pm 14$  and  $276 \pm 14$  kJ mol<sup>-1</sup>, respectively, are in close agreement, and that the mean value of  $n$  is  $\approx 1$ , which is indicative of a surface growth crystallization mechanism [34, 35].

To study the nature of the crystallization process, the change of the fraction of crystallization ( $\chi$ ) with temperature ( $T$ ) for different heating rates was evaluated, and the typical sigmoid curves that were obtained (see Fig. 7) suggest that the formation of the crystalline phase proceeded by a combination of nucleation and growth processes [36]. The results on change of the crystallization rate ( $d\chi/dt$ ) with  $T$ , shown in Fig. 8, reveal that the value of the

maximum crystallization rate, corresponding to the peak temperature of crystallization,  $(d\chi/dt)_{T_p}$ , increases with the increase in the heating rate, as it has been reported in the literature for different types of glasses [12, 23, 24].

Considering that the plot of  $\ln[-\ln(1-\chi)]$  versus  $1,000/T$  should be a straight line with a slope equal to  $1.052(n-1)E_c/R$ , according to modified Ozawa equation [25], Eq. (8), and that in the present work non-linear plots were obtained, as shown in Fig. 9, it is suggested that there is a variation of  $E_c$  and of  $n$  during the whole crystallization process of the glass [26]. Generally, activation energy is defined as the threshold energy above which a transformation takes place, and for each particular transformation, it should have a characteristic and constant value. However, it has been observed that in some glass systems, the activation energy is dependent on the fraction of crystallization,  $\chi$ , [26, 29]. Therefore, in the present work, it was considered interesting to study the change of the activation energy and of Avrami exponent during the crystallization of the glass at the various heating rates. So, an effective activation energy,  $E_c(\chi)$ , was considered, which reflects the change of nucleation and growth behavior during the crystallization process.

From the results presented in Fig. 11, it is noticed that for a fixed  $\chi$  value, the value of  $E_c(\chi)$  obtained according to Eq. (9) is  $\sim 15 \text{ kJ mol}^{-1}$  lower than that obtained according to Eq. (10), and that  $E_c(\chi)$  decreases slightly in the initial stages of crystallization ( $\chi < 0.3$ ); it is constant in the range  $0.3 < \chi < 0.6$ , and then it decreases for higher  $\chi$  values. The values of  $E_c(\chi)$  calculated for the entire crystallization fraction range (decreasing from  $\sim 370$  to  $\sim 310 \text{ kJ mol}^{-1}$ ) are higher than  $E_c$  values determined according to Eqs. (5) and (6),  $\sim 262$  and  $\sim 276 \text{ kJ mol}^{-1}$ , respectively, quoted in Table 1.

The effective activation energy  $E_c(\chi)$  may be considered as composed of two parts: the activation energy of nucleation ( $E_n$ ), and the activation energy of growth ( $E_g$ ) [12, 37]. This could be expressed as [12]

$$E_c(\chi) = aE_n + bE_g, \quad (12)$$

where  $a$  and  $b$  are the two variables related to the Avrami parameter, and  $a + b = 1$ . It is expected that at the beginning, the process of nucleation dominates ( $b = 0$ ), and at the end of the crystallization, only the growth process ( $a = 0$ ) is expected to dominate [12]. For the exothermic peak, as  $\chi \rightarrow 0$ ,  $E_c(\chi) \rightarrow E_n \approx 370 \text{ kJ mol}^{-1}$  and as  $\chi \rightarrow 1$ ,  $E_c(\chi) \rightarrow E_g \approx 310 \text{ kJ mol}^{-1}$ .

From Fig. 11, where the change of the Avrami exponent with the fraction of crystallization ( $\chi$ ) is shown, it is observed that the local Avrami exponent increases from  $n \approx 0.8$  to 1.0 with the increase in the fraction of crystallization. Allowing for the experimental error, the mean

value of  $n$  is considered close to 1 indicating a surface crystallization mechanism [34, 35].

### Crystal phase development and microstructure

In glass-plate samples, treated at a temperature below the onset of the DTA exothermic peak, no evidence of crystalline phase formation was found by XRD analysis. However, after heating the glass samples during 8 h at 733 K—a temperature between  $T_g$  and the onset of the exothermic peak—followed by a treatment for 2 h at 773 K—a temperature within the exothermic peak and below  $T_p$ —aluminum metaphosphate,  $\text{Al}(\text{PO}_3)_3$ , was identified as the predominant phase, together with a secondary phase, aluminum phosphate ( $\text{AlPO}_4$ ), as shown in Fig. 12b. After heating the samples for 8 h at 733 K followed by a treatment for 2 h at 873 K, a temperature above  $T_p$ , aluminum metaphosphate,  $\text{Al}(\text{PO}_3)_3$  was identified as the predominant phase, together with other minor phases (aluminum phosphate,  $\text{AlPO}_4$ , barium phosphate,  $\text{Ba}_2\text{P}_2\text{O}_7$ , and barium-aluminum phosphate,  $\text{Ba}_3\text{AlPO}_7$ ), as presented in Fig. 12c.

The as-prepared glass and heat-treated glass samples have been further characterized using optical microscopy and SEM to confirm the isotropic/anisotropic nature of the samples and to analyze the crystal morphology. The optical microscopy image presented in Fig. 13a appears dark, revealing the isotropic nature of the glass. The optical image of the glass heat treated during 8 h at a temperature  $T$  between the endothermic peak and the exothermic peak ( $T = 733 \text{ K}$ ) was also dark due to the isotropic nature of the glass matrix and of the clusters formed in the glass matrix. The existence of these clusters in the glass surface, having an average size of  $1 \mu\text{m}$ , is shown in the SEM image presented in Fig. 14a. A glass sample heat treated at 733 K for 8 h followed by a treatment at 773 K for 2 h, which looked as a transparent sample, when observed by optical microscopy resulted in an image such as that presented in Fig. 13b, exhibiting a dark area corresponding to the isotropic glass matrix that contained an anisotropic bright crystal. The glass sample heated under such conditions, when observed by SEM, showed the microstructural features revealed by the micrograph presented in Fig. 14b, where a uniform glass matrix containing some spherulitic shape crystals grown from the surface is visible. A spherulite structure consisting of confocal arrays of fine fibrillar crystals which grow with preferred radial orientation has been considered, when the glass crystallization rates are very slow [24]. The microstructural observations indicated that the formation of the crystallites takes place from the surface of the glass samples, confirming the above results on the evaluation of the Avrami exponent by non-

isothermal analysis that points out for a surface crystallization mechanism ( $n \approx 1$ ).

The optical image of a sample heat treated at 733 K for 8 h followed by a treatment at 873 K for 2 h, which showed already some turbidity, is shown in Fig. 13c. Apart from the appearance of an exaggerated anisotropic bright crystal, it is verified that the sample is fully crystallized, containing small crystals, which have a spherulitic shape as can be observed in the SEM micrograph shown in Fig. 14c. The presence of aluminum metaphosphate as the predominant crystalline phase in the crystallized glass was confirmed by SEM/EDS. It is clearly envisaged in EDS elemental mapping (Fig. 15) that the crystals consist mainly of Al, P, and O, corresponding to the aluminum phosphate phase. Except lithium, which is not detected for being a lighter element, the remaining elements (Ba, La, and Tb) contained in the glass composition are uniformly distributed.

Aluminophosphate-based glasses and glass ceramics can be used in various optical applications, particularly as laser host materials [38]. It has been demonstrated that microporous and mesoporous aluminophosphate materials containing RE ions have potential applications in catalysis, phosphors, lasers, optical amplifiers, fibers, and optical memories [39]. A future extension of the present study will be the investigations on the synthesis and characterization of RE-doped aluminophosphate glass ceramics for application in optoelectronics as optical amplifiers.

## Conclusions

The glass transition temperature and the peak crystallization temperature were related to the heating rate according to the Lasocka equation. The values of the activation energy for glass transition determined by two different methods were  $462 \pm 14$  and  $475 \pm 14$  kJ mol<sup>-1</sup>. The crystallization parameters of the glass, which are scientifically important, have been evaluated using different methods derived from non-isothermal experiments. The average value of the activation energy for crystallization was  $262 \pm 14$  and  $276 \pm 14$  kJ mol<sup>-1</sup> for the Kissinger and Ozawa methods, respectively. The change of the activation energy for crystallization with the fraction of crystallization was evaluated, and it was verified that it decreased slightly from  $\sim 370$  to  $\sim 310$  kJ mol<sup>-1</sup> with the increase in the fraction of crystallization from 0.1 to 0.9. The mean value of the Avrami exponent was close to 1, indicating a surface crystallization process. This was confirmed by the microstructural analysis of the heat-treated samples where the formation of spherulitic crystals identified as aluminum phosphate was observed.

**Acknowledgements** Andreia Lopes for help with DTA tests. Financial support for the work was given by Foundation for Science and Technology–Portugal (ERA-MNT/001/2010 and PEst-C/CTM/LA0025/2013 projects), and by Executive Unity for Financing of Higher Education, Research and Innovation–Romania (7-031/2011 MNT-ERA.NET contract and 168/2012 Project from Partnership Program).

## References

- Weber MJ, Saroyan RA, Ropp RC (1981) Optical properties of Nd<sup>3+</sup> in metaphosphate glasses. *J Non-Cryst Solids* 44:137–148
- Paulose PI, Jose G, Thomas V, Unnikrishnan NV, Warriar MKR (2003) Sensitized fluorescence of Ce<sup>3+</sup>/Mn<sup>2+</sup> system in phosphate glass. *J Phys Chem Solids* 64:841–846
- Nogami M, Enomoto T, Hayakawa T (2002) Enhanced fluorescence of Eu<sup>3+</sup> induced by energy transfer from nanosized SnO<sub>2</sub> crystals in glass. *J Luminescence* 97:147–152
- Elisa M, Sava BA, Vasiliu IC, Monteiro RCC, Veiga JP, Gherghe L, Feraru I, Iordanescu R (2013) Optical and structural characterization of samarium and europium-doped phosphate glasses. *J Non-Cryst Solids* 369:55–60
- Nico C, Graça MPF, Elisa M, Sava BA, Monteiro RCC, Rino L, Monteiro T (2013) Effects of ultraviolet excitation on the spectroscopic properties of Sm<sup>3+</sup> and Tb<sup>3+</sup> doped aluminophosphate glasses. *Opt Mater* 35:2382–2388
- Nico C, Fernandes R, Graça MPF, Elisa M, Sava BA, Monteiro RCC, Rino L, Monteiro T (2014) Eu<sup>3+</sup> luminescence in aluminophosphate glasses. *J Luminescence* 145:582–587
- Chonggeng MA, Jiang S, Zhou X (2010) Energy transfer from Ce<sup>3+</sup> to Tb<sup>3+</sup> and Eu<sup>3+</sup> in zinc phosphate glasses. *J Rare Earths* 28:40–42
- Dongbing H, Chunlei Y, Jimeng C, Li S, Hu L (2011) Energy transfer between Gd<sup>3+</sup> and Tb<sup>3+</sup> in phosphate glass. *J Rare Earths* 29:48–51
- Abdel-Hameed SA, Ghoniem NA, Saad EA, Margha FH (2005) Effect of fluoride ions on the preparation of transparent glass ceramics based on crystallization of barium borates. *Ceram Int* 31:499–505
- Ghasemzadeh M, Nemati A, Baghshahi S (2012) Effects of nucleation agents on the preparation of transparent glass-ceramics. *J Eur Ceram Soc* 32:2989–2994
- Fang Y, Liao M, Hua L (2006) Effect of lithium–sodium mixed-alkali on phase transformation kinetics in Er<sup>3+</sup>/Yb<sup>3+</sup> co-doped aluminophosphate glasses. *Thermochim Acta* 443:179–182
- Majhi K, Varma KB (2009) Crystallization kinetic studies of CaBi<sub>2</sub>B<sub>2</sub>O<sub>7</sub> glasses by non-isothermal methods. *J Mater Sci* 44:385–391
- El-Salam A, Abousehly M (1996) Activation energy of Se<sub>2</sub>-Ge<sub>0.2</sub>Sb<sub>0.8</sub> chalcogenide glass by differential scanning calorimetry. *J Therm Anal Calorim* 46:177–186
- Starink MJ, Zahra A (1997) Determination of the transformation exponents from experiments at constant heating rate. *Thermochim Acta* 298:179–189
- Johnson WA, Mehl RF (1939) Reaction kinetics in processes of nucleation and growth. *Trans AIME* 135:416–442
- Avrami M (1940) Kinetics of phase change. II transformation-time relations for random distribution of nuclei. *J Chem Phys* 8:212–224
- Avrami M (1941) Kinetics of phase change. III granulation, phase change, and microstructure. *J Chem Phys* 9:177–184
- Sava BA, Elisa M, Boroica L, Monteiro RCC (2013) Preparation method and thermal properties of samarium and europium-doped aluminophosphate glasses. *Mater Sci Eng B* 178:1429–1435

19. Lasocka M (1976) The effect of scanning rate on glass transition temperature of sput-cooled  $\text{Te}_{85}\text{Ge}_{15}$ . *Mater Sci Eng* 23:173–177
20. Kissinger HE (1956) Variation of peak temperature with heating rate in differential thermal analysis. *J Res Natl Bur Stand* 57:217–221
21. Mahadevan S, Giridhar A, Singh AK (1986) Calorimetric measurements on As–Sb–Se glasses. *J Non-Cryst Solids* 88:11–34
22. Ozawa T (1971) Kinetics of non-isothermal crystallization. *Polymer* 12:150–158
23. Vásquez J, Wagner C, Villares P, Jiménez-Garay R (1998) Glass transition and crystallization kinetics in  $\text{Sb}_{0.18}\text{As}_{0.34}\text{Se}_{0.48}$  glassy alloy by using non-isothermal techniques. *J Non-Cryst Solids* 235:548–553
24. Arora A, Shaaban ER, Singh K, Pandey OP (2008) Non-isothermal crystallization kinetics of  $\text{ZnO-BaO-B}_2\text{O}_3\text{-SiO}_2$  glass. *J Non-Cryst Solids* 354:3944–3951
25. Matusita K, Komatsu T, Yokota R (1983) Kinetics of non-isothermal crystallization process and activation energy for crystal growth in amorphous materials. *J Mater Sci* 19:291–296
26. Lu K, Wang JT (1991) Activation energies for crystal nucleation and growth in amorphous alloys. *Mater Sci Eng A* 133:500–503
27. Friedman HL (1965) Kinetics of thermal degradation of char-forming plastics from thermogravimetry. Application to a phenolic plastic. *J Polym Sci Part C* 6:183–195
28. Ozawa T (1970) Kinetic analysis of derivative curves in thermal analysis. *J Therm Anal* 2:301–324
29. Lu W, Yan B, Huang W (2005) Complex primary crystallization kinetics of amorphous Finemet alloy. *J Non-Cryst Solids* 351:3320–3324
30. Rabinal MK, Sangunni KS, Gopal ES (1995) Chemical ordering in  $\text{Ge}_{20}\text{Se}_{80-x}\text{In}_x$  glasses. *J Non-Cryst Solids* 188:98–106
31. Mehta N, Kumar A (2005) Applicability of Kissinger's relation in the determination of activation energy of glass transition process. *J Optoelect Adv Mater* 7:1473–1478
32. Imran MM, Bhandari D, Saxena NS (2001) Enthalpy recovery during structural relaxation of  $\text{Se}_{96}\text{In}_4$  chalcogenide glass. *Phys B. Cond Matter* 293:394–401
33. Agarwal P, Goel S, Rai JS, Kumar A (1991) Calorimetric studies in glassy  $\text{Se}_{80-x}\text{Te}_{20}\text{In}_x$ . *Phys Status Solid A* 127:363–369
34. Erol M, Kuchukbayrak S, Ersoy-Mericboyu A (2009) The application of differential thermal analysis to the study of isothermal and non-isothermal crystallization kinetics of coal fly ash based glasses. *J Non-Cryst Solids* 355:569–576
35. Ghasemzadeh M, Nemati A, Golikand AN, Hamnabard Z, Baghshahi S (2011) Utilization of DTA in the determination of a crystallization mechanism in transparent glass-ceramics with a nanocrystalline structure. *Synth React Inorg Metal-Org Nano-Metal Chem* 41:561–570
36. Jean J, Fang Y, Dai SX, Wilcox DL Sr (2001) Devitrification kinetics and mechanism of  $\text{K}_2\text{O-CaO-SrO-BaO-B}_2\text{O}_3\text{-SiO}_2$  glass-ceramic. *J Am Ceram Soc* 84:1354–1360
37. Yinnon H, Uhlmann DR (1983) Applications of thermoanalytical techniques to the study of crystallization kinetics in glass-forming liquids, part I: theory. *J Non-Cryst Solids* 54:253–275
38. Weber MJ (1990) Science and technology of laser glass. *J Non-Cryst Solids* 123:208–222
39. Yan W, Zhang Z, Xu J, Mahurin SM, Dai S (2005) Doping of rare earth elements into microporous and mesoporous aluminophosphate. *Stud Surf Sci Catal* 156:265–272